Nitrogen Fixation by Gliding Arc Plasma: Better Insight by Chemical Kinetics Modelling

Weizong Wang,*[a]Bhaskar Patil,[b]Stjin Heijkers,[a]Volker Hessel,[b] and Annemie Bogaerts*[a]

Abstract: The conversion of atmospheric nitrogen into valuable compounds, i.e., so-called nitrogen fixation, is gaining increasing interest, owing to the essential role in the nitrogen cycle of the biosphere. Plasma technology, and more specifically a gliding arc plasma, has great potential in this area, but little is known about the underlying mechanisms. Therefore, we performed a detailed chemical kinetics modelling for a pulsed power gliding arc reactor operating at atmospheric pressure for nitrogen oxide synthesis. Experiments are carried out to validate the model and reasonable agreement is reached between the calculated and measured NO and NO_2 yields and the corresponding energy efficiency for NO_x formation for different N_2/O_2 ratios, indicating that the model can provide a realistic picture of the plasma chemistry. Therefore, we can use the model to investigate the reaction pathways for the formation and loss of NO_x. The results indicate that vibrational excitation of N_2 in the gliding arc contributes significantly to activating the N_2 molecules, and leads to an energy efficient way of NO_x production, compared to the thermal process. Based on the underlying chemistry, the model allows us to propose solutions on how to further improve the NO_x formation by gliding arc technology. Although the energy efficiency of gliding arc based nitrogen fixation process at present stage is not comparable to the world-scale Haber–Bosch process, we believe our study helps us to come up with the more realistic scenarios of entering a cutting-edge innovation in new business cases of the decentralized production of fertilizer for agriculture which are essentially opened by the intrinsic potential of low-temperature plasma technology.

[a] *Dr. W.Z Wang, S.Heijkers, Prof.Dr. A. Bogaerts*
Department of Chemistry, research group PLASMANT
University of Antwerp
Universiteitsplein 1, 2610 Antwerp (Belgium)
E-mail: wangweizong@gmail.com
annemie.bogaerts@uantwerpen.be

[b] *B. Bhaskar, Prof. Dr. V. Hessel*
Department of Chemical Engineering and Chemistry, Laboratory of Chemical Reactor Engineering / Micro Flow Chemistry and Process Technology
Eindhoven University of Technology
P. O. Box 513, 5600 MB Eindhoven (The Netherlands)

Supporting information for this article is given via a link at the end of the document.

Introduction

Nitrogen is an essential component for all forms of life because it is required to biosynthesize basic building blocks of plants and living organisms. The latter can consume nitrogen in a usable form, obtained by chemical reaction with oxygen or hydrogen or carbon. Therefore, we find nitrogen compounds in plant cells, amino acids, proteins and nucleic acids. In the earth's atmosphere, there is an abundant supply of nitrogen – 78.08% of the gas is composed of molecular nitrogen (N_2). However, this most abundant nitrogen source is not available to the majority of living organisms because it is extremely difficult to break the triple bond and the very stable electronic configuration, which make almost any first reaction step of the conversion very energy demanding. As a result, nitrogen fixation (**NF**), which converts nitrogen molecules into simple nitrogen compounds, such as ammonia or nitric oxide that can be further used as precursors for the synthesis or biosynthesis of more complex molecules, is very significant. However, it is the most challenging step of nitrogen utilization by living organisms.[1]

The conventional Haber–Bosch (H-B) process of the binding of nitrogen with hydrogen to produce ammonia at high pressure and temperature is the most significant process to produce fertilisers.[2] It is expected that the global ammonia capacity will increase from 204.2 million tons per year in 2013 to 249.4 million tons by 2018.[3] Hence, the amount of synthetic nitrogen obtained by human activities has exceeded natural biological fixation.[4] From an energy point of view, industrial ammonia synthesis is the most energy intensive chemical process. The H–B process consumes 1–2 % of the world's total energy production and utilizes 2-3 % of the total natural gas output. Furthermore, it emits more than 300 million metric tons of carbon dioxide.[5]-[6]

Considering the increasing demand of fertilizers, the high energy intensity and environmental concerns triggered by industrial nitrogen fixation (i.e., the H–B process), the need to develop and integrate more sustainable processes becomes imperative.[7]-[8] Several alternative (non-conventional) technologies are being investigated, such as biological NF,[9]-[10]and NF with metallocomplex homogeneous catalysts under ambient pressure.[11] Another new technology considered to have great potential for reducing the environmental impact and improving the energy efficiency is based on plasma, i.e., an ionized gas,

typically created by applying electric energy. Especially when sustainable energy sources such as wind and solar cells are utilized for the generation of electricity, the dependence on fossil fuels during this industrial process is greatly reduced and no greenhouse gas emissions take place. This makes plasma an inherent “green” technology.

Plasma based NF is generally accomplished by the reaction of nitrogen with oxygen or hydrogen to produce nitrogen oxide (nitric oxide) or ammonia, respectively.[1] For plasma based ammonia synthesis, expensive hydrogen is required, besides readily available nitrogen. In contrast, for plasma based nitric oxide synthesis, the raw materials (air) are abundantly available at low cost. As a result, more research devoted to the plasma based nitric oxide synthesis can be found in the literature.[12]-16] For this purpose, either thermal or non-thermal plasma can be used. Thermal plasma, however, requires very high temperatures and the energy efficiency is low. Non-thermal plasma, on the other hand, is very promising, because the theoretical limit of the energy consumption of nitrogen oxidation is more than 2.5 times lower than that of the H–B process.[16]Thus, atmospheric non-thermal plasmas offer unique perspectives because of their capacity to induce chemical reactions within gases with a limited energy cost at ambient pressure and temperature.

Gliding arc plasmas are among the most effective and promising plasmas for gas conversion,[17]-30] because they offer benefits of both thermal and non-thermal discharges. They are typically considered as ‘warm’ discharges, and vibrational excitation of the molecules is seen as the most efficient way to assist the conversion or synthesis.[31] A few studies have been reported on employing a gliding arc reactor for nitrogen fixation.[32]-38]The highest concentration of NO_x achieved was found to be 1.0 % in a milli-scale gliding arc reactor.[37] In this reactor, one can expect to benefit from an intensified contact of the reactive plasma species with the gas molecules, and therefore a higher efficiency in delivering energy to the reactant gases.

In order to improve the applications (i.e., mainly gas conversion), the physical and chemical characteristics of the gliding arc have been extensively studied by both experiments[39]-44]and computer modelling [45]-59]. The latter is very useful in providing more insight into the underlying reaction mechanisms of plasma assisted gas conversion or synthesis, e.g. by evaluating quantities which are difficult to measure, and by identifying the most important chemical reactions or parameters.[45]-51] However, only a few papers in literature deal with modelling of a gliding arc.[52]-59] To our knowledge, there exist no models yet for NO_x synthesis in a gliding arc.

Previous theoretical analysis has revealed that vibrationally excited nitrogen plays an important role in energy efficient NO formation,[16], [38] but these studies lack a description of the plasma chemistry. For N_2/O_2 mixtures, several papers have presented kinetic models with a complex description of the vibrational and electronic levels,[60]-64] but these models do not apply to a gliding arc reactor. As a result, the various mechanisms that contribute to NO_x production in a gliding arc are not yet completely understood. This may be because a gliding arc is a non-stationary discharge and its effective volume is changing due to the arc elongation caused by the gas blast. Therefore, building an accurate model for such a non-uniform reactor with a complex plasma chemistry is very challenging.

In this paper, for the first time, we study the NO_x synthesis in a pulsed power gliding arc reactor by a chemical kinetics model. Experiments are performed to benchmark the model. We investigate the product yields of various NO_x compounds, the reaction selectivity and the energy efficiency, for different feed ratios of N_2/O_2. By comparing these values with those for the pure thermal process, where most of the energy is spent on the gas heating rather than on the nitrogen oxidation reactions, we can clearly demonstrate the non-equilibrium character of the gliding arc and explain the higher values of the NO_x yield and energy efficiency. Furthermore, in order to increase our general understanding of the underlying mechanisms and pathways, we perform a kinetic analysis, based on the simulation results, to elucidate the role of various plasma species, and especially of the N_2 vibrational states, in the NO_x synthesis. This enables us to propose solutions on how to further improve the formation of NO_x by gliding arc technology.

Results and Discussion

NO_x formation

The measured and calculated NO and NO_2 concentrations are plotted as a function of N_2/O_2ratio in the gas mixture in figure 1 (a,b). The total NO_X concentration (i.e., sum of NO + NO_2) and the NO and NO_2 selectivity are presented in figure 2 (a,b). Note that the experiments are limited to a N_2/O_2 ratio in the range of 0.25 – 4, while the simulations are performed in a wider range of 0.025 – 40, to obtain additional information. The concentrations of NO and NO_2 follow a similar parabolic trend upon varying the N_2/O_2 ratio, and there exists an optimum feed ratio at which the maximum yield is reached. This is logical, because both N_2 and O_2 are the (initial) precursors for NO and NO_2. Experimentally the concentration of NO increases until a feed ratio of 3, after which the NO concentration starts to decline. The NO_2 concentration reaches its peak at a feed ratio of 1. The calculated results follow a left-skewed trend for both NO and NO_2, as well as for their sum, with respect to the experimental values. However, the absolute values of the calculated and measured concentrations are in rather good agreement, certainly in view of the complexity of the plasma chemistry.

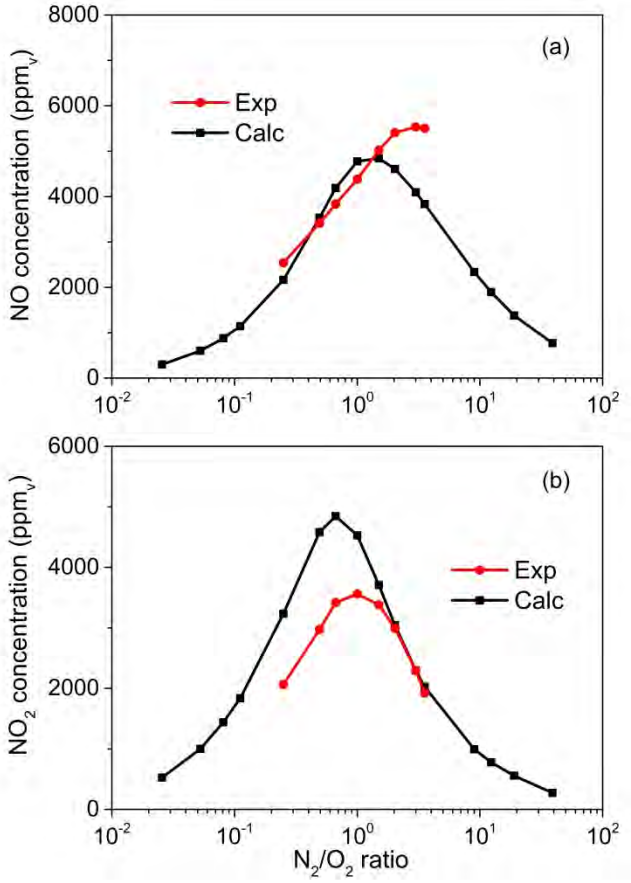

Figure 1. Experimental and calculated concentrations of NO (a) and NO_2 (b)as a function of the N_2/O_2 ratio in the feed gas, for a gas flow rate of 2 L/min and a SEI of 1.4 kJ/L (or 0.35 eV/molec).

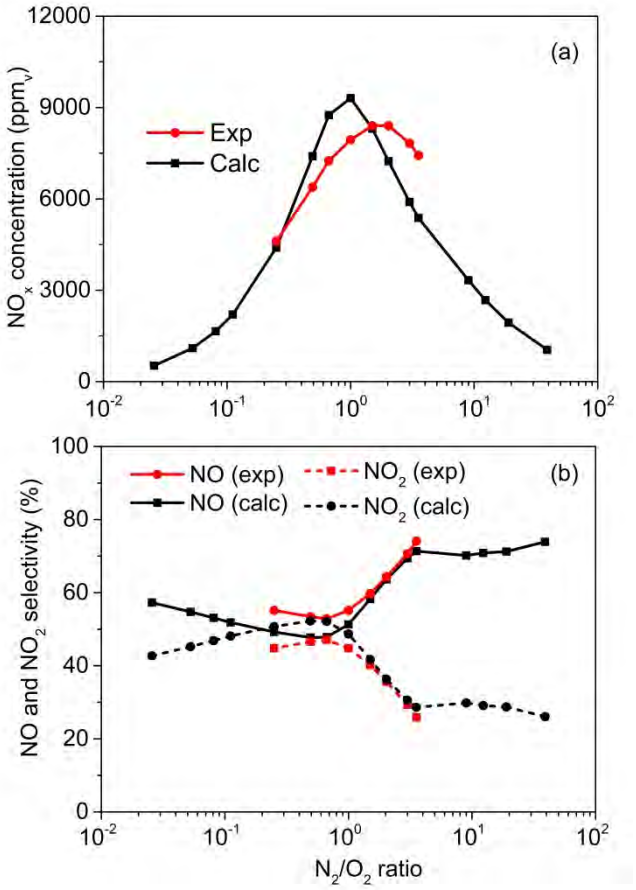

Figure 2. Experimental and calculated concentrations of NO_X (taken as NO + NO_2) (a) and NO and NO_2 selectivity (d) as a function of the N_2/O_2 ratio in the feed gas, for a gas flow rate of 2 L/min and a SEI of 1.4 kJ/L (or 0.35 eV/molec).

At a feed ratio of N_2/O_2 around 1, both the NO and NO_2 selectivity are close to 50 %, but at a higher feed ratio, both the experimental and calculated NO selectivity increase, while the NO_2 selectivity shows the opposite trend. This is logical, because NO_2 production by NO oxidation becomes less important upon increasing fraction of N_2. When the feed ratio of N_2/O_2 is below 1, the NO selectivity again increases slightly, and the calculated value reaches about 60 % at a low N_2/O_2 ratio around 0.02, while the calculated NO_2 selectivity is only 40 %. This is because the net formation rate of NO_2 decreases more than that of NO with increasing O_2fraction. In general we can conclude that reasonable agreement is obtained between the experimental and calculated data, indicating that the model can provide a more or less realistic picture of the plasma chemistry, and can thus be used to elucidate the underlying mechanisms, as will be shown later.

Comparison of our results with thermal NO_x formation and with the Haber-Bosch process

In order to evaluate the performance of our gliding arc for nitrogen fixation, we compare our results with the thermal NO_x yield, calculated as a function of gas temperature (See the calculation method in the supporting information). The thermal NO_x yield model is based on the chemical equilibrium composition which is calculated by finding the composition that minimizes the Gibbs free energy. It is a standard technique in equilibrium chemistry and used widely in the literature due to the difficulties in performing related experiments at a very high temperature.[65]

Figure 3 shows the calculated equilibrium species composition of a 50% N_2/50% O_2 mixture, as a function of the gas temperature at atmospheric pressure. At room temperature, the thermal NO_x (i.e., NO + NO_2) yield is negligible because the species energy is not high enough to break the nitrogen bond. With increasing gas temperature, the molar fractions of NO and NO_2 increase. The selectivity of NO is higher than that of NO_2due to the dissociation of NO_2 into NO and O at higher temperature. The concentration of NO reaches a peak at around

3500 K. A further temperature increase yields a reduction of the NO yield, because of dissociation of NO into N and O atoms.

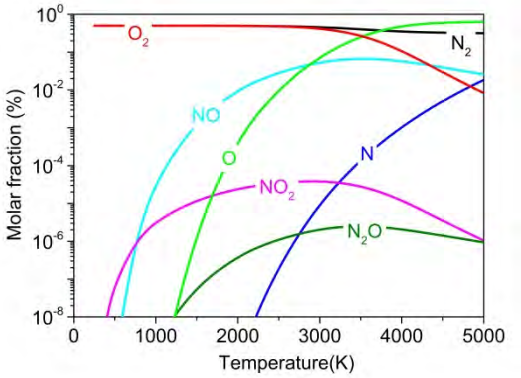

Figure 3. Calculated gas composition for a 50% N_2/ 50% O_2 mixture, as a function of the gas temperature at atmospheric pressure.

The variations in molar fractions of NO and NO_2 as a function of temperature explain why the thermal NO_x yield and corresponding energy efficiency both show a peak at a certain temperature, as illustrated in figure 4. Our calculations predict the highest thermal NO_x yield of approximately 8 % at 3500 K. The corresponding energy efficiency is then about 2.9 %. At 3000 K, a somewhat higher energy efficiency of nearly 4 % is reached, but the NO_x yield is then only 5.5 %. The reason that a higher energy efficiency is reached at a somewhat lower temperature is simply because a lower SEI is needed, as is obvious from the dashed curve in figure 4.

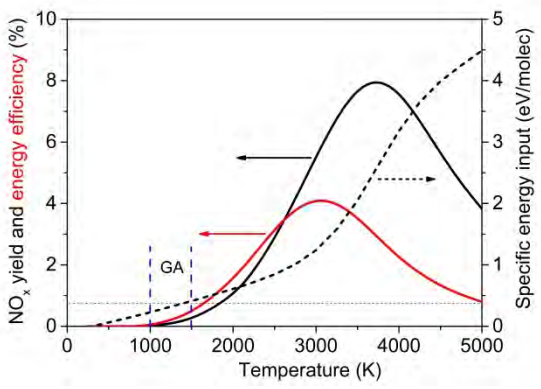

Figure 4. Calculated thermal NO_x yield (solid black line, left y-axis) and corresponding energy efficiency (solid red line, left y-axis), as well as the corresponding specific energy input (dashed line, right y-axis), as a function of gas temperature for a 50% N_2 / 50% O_2 mixture at atmospheric pressure. The typical gas temperature range in our gliding arc is indicated with the blue vertical dashed lines.

In figure 4, we also indicate the typical gas temperature range in our gliding arc; see the blue vertical dashed lines. The thermal NO_x yield is only about 0.16 % at 1500 K, which is the highest gas temperature in our gliding arc. Because only a limited fraction (around 7.8 %; cf. Supporting information) of the total gas flowing into the reactor during every gliding arc cycle is processed by the effective gliding arc volume, the thermal NO_x yield of 0.16 % would correspond to an overall NO_x yield of only 25 ppm_v, which is a factor 320 lower than the value of nearly 8000 ppm_v that we measured in our gliding arc (cf. figure 2(a)). Furthermore, if all the gas flowing into the reactor would be treated by the thermal process, an SEI of 1.4 kJ/L (or 0.35 eV/molec) would lead to an overall NO_x yield around 1095 ppm_v, which is still much lower than our measured value. This low NO_x concentration obtained by the thermal process demonstrates that most of the energy is spent on gas heating rather than on nitrogen oxidation, and that our gliding arc clearly operates in non-equilibrium conditions, explaining the much higher NO_x yield.

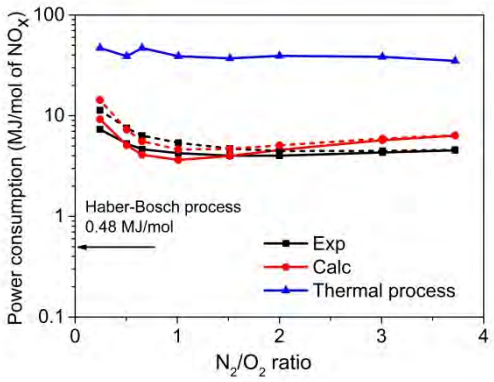

Figure 5. Experimental and calculated energy consumption of NO_x formation as a function of the N_2/O_2 ratio in the mixture, for a gas flow rate of 2 L/min and a SEI of 1.4 kJ/L (or 0.35 eV/molec), and comparison with the thermal process at the same SEI value. Solid lines: without the energy cost of gas preparation, dashed lines: with the energy cost of gas preparation. The energy consumption of the Haber–Bosch (H–B) process is also presented for comparison.

The experimental and calculated energy consumption per mole of NO_x formed with and without including the energy cost of gas preparation is plotted in figure 5 as a function of the N_2/O_2 ratio. At low N_2/O_2 ratios, only considering the plasma energy consumption, the energy required for NO_x formation slightly decreases with increasing N_2/O_2 ratio, up to a value of 37.1 MJ/mol at a N_2/O_2 ratio of 1, after which the experimental value remains constant, while the calculated value slightly increases again upon higher N_2/O_2 ratios. This is logical because the N_2/O_2 ratio around 1 gives rise to the highest calculated NO_x concentration. As indicated in figure 5, the consumption of NO_x formation including the energy cost of gas preparation shows a quite similar trend with the variations of the N_2/O_2 ratios. The influence of the energy cost of gas preparation on the total energy consumption gradually decreased with an increasing N_2 content. This is because the pure oxygen flow rate and hence the related energy cost of gas preparation decreases. With a feeding ratio of 79% N_2 / 21% O_2, air as the only feed gas was found to produce a slightly lower amount of NO_x than the mixture with the optimized N_2/O_2 feed ratio of around 1.0 for which more energy is needed to prepare the pure gas and this definitely brings the cost benefits, i.e. a relatively lower total energy consumption as indicated in figure 5.

The current industrial scale Haber–Bosch process provides a benchmark of the energy consumption for plasma based N-fixation processes. The energy requirement for the Haber–

Bosch process is much lower, i.e. 0.48 MJ/mol of N atoms.[66] This value includes the energy consumption during the whole industrial production process of ammonia using three main raw materials: natural gas, air and water. Current comparison indicates that plasma based N-fixation is not yet competitive with the industrial H-B process, which operates of course on a much larger scale. Hence, it is obvious that much more research is needed to further improve the plasma based N-fixation process. On the other hand, it is also clear from figure 5 that the gliding arc requires about 10 times less energy than the thermal process of NO_x formation, calculated with the same energy input of 1.4 kJ/L (or 0.35 eV/molec). Due to the high temperature challenge in establishing thermal plasma discharge in gliding arc reactors, it is difficult to validate our thermal NO_x yield model by direct comparison with the experiments under specific conditions. However, literature experimental work[67]-71] via other thermal plasma reactor which our thermal conversion model is applicable generally brings a higher energy consumption of NO_x synthesis than our current work because the energy in a thermal system is distributed over all degrees of freedom, including those not effective for the NO_x synthesis. This is in reasonable agreement with the prediction of our thermal NO_x yield model although it is not easy to compare different reactor setups with different discharge conditions.

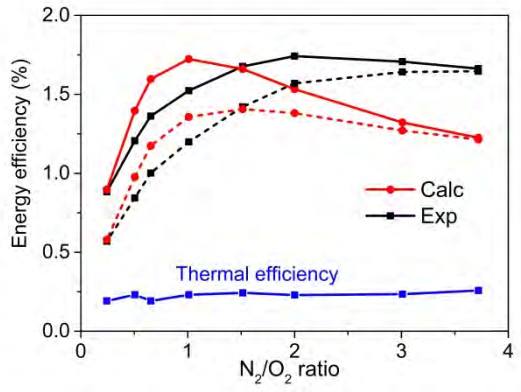

Figure 6.Experimental and calculated energy efficiency of NO_x formation as a function of the N_2/O_2 ratio in the mixture, for a gas flow rate of 2 L/min and a SEI of 1.4 kJ/L (or 0.35 eV/molec), and comparison with the thermal energy efficiency at the same SEI value. Solid lines: without the energy cost of gas preparation, dashed lines:with the energy cost of gas preparation.

The fact that the energy efficiency of the gliding arc for NO_x synthesis is much better than that for the thermal process can also be deduced from figure 6. Indeed, both the calculated and measured energy efficiency with and without considering the energy cost of gas preparation are around 0.5-1.7 %, whereas the thermal energy efficiency calculated for the same SEI of 1.4 kJ/L is only about 0.2 %. Hence, this clearly demonstrates the non-equilibrium character of the gliding arc for NO_x synthesis, i.e., the NO_x synthesis does not proceed thermally, but upon electron induced processes, contributing to energy efficient chemical reactions, as will be explained below. Moreover, including the energy cost related to the gas preparation, the experimental energy efficiency using air shows the highest value under different feed ratios although addition of oxygen to air slightly enhanced the production of NO_x to some extent. This once again shows a cheap and readily available atmospheric pressure air is suited and preferred than pure N_2+O_2 mixture.

Underlying mechanisms of NO_x formation in the GA: energy efficient process by vibrational excitation of N_2

As mentioned above, the NO_x formation in our gliding arc, as well as in other types of plasmas, is induced by electron impact reactions with the N_2 and O_2 molecules. In figure 7, we illustrate how the electron energy is transferred to different channels of excitation, ionization and dissociation of both N_2 and O_2molecules in a 50% N_2 / 50% O_2 mixture, as a function of the reduced electric field (E/n) in the discharge. This reduced electric field is an important parameter to distinguish different plasma types, as it determines the average electron energy in the plasma, and thus the rate of the various electron impact reactions. The electron energy values corresponding to the reduced electric field values are thus also indicated in figure 7 (see top and bottom x-axes). A GA is typically characterized by reduced electric field values between 5 and 100 Td (see the vertical dashed lines in figure 7), while a dielectric barrier discharge (DBD), which is a quite popular type of plasma for gas conversion applications, typically operates at higher values than 100 Td.[31] Note that 1 Td corresponds to 10^{-21} V m^2.

It is known that the energy efficiency of NO_x formation is determined by the method to break the strong (~10 eV) bond of the N_2 molecule. Above approximately 100 Td, as we can see from figure 7, most electron energy goes into electronic excitation, dissociation and ionisation of the N_2 (and O_2) molecules. The N atoms produced by direct electron impact dissociation of N_2 molecules can react with O_2 molecules to form NO. However, due to the very high dissociation threshold level of N_2, the energy efficiency in this case would be limited to a low level of about 3 %.[31] This explains why a DBD is characterized by a lower energy efficiency, or a higher energy consumption for NO_x synthesis, as we will illustrate further in this paper. We can describe this mechanism as follows,

$$e + N_2 \rightarrow N_2(a^1\Pi_g)\ ,\ N_2(B^3\Pi_g),\ N_2(b^1\Pi_u) + e \rightarrow e + N + N \quad (1)$$

$$N + O_2 \rightarrow NO + O,\ E_a \approx 0.3 \text{ eV/molec},\ \Delta H \approx -0.94 \text{ eV/molec} \quad (2)$$

On the other hand, in the reduced electric field range lower than 100 Td, which is characteristic for our gliding arc, electron impact vibrational excitation of N_2 is the dominant electron process, as is clear from figure 7, and the resulting N_2 molecules in vibrational levels will be important for NO formation in our case. Indeed, the relatively high energy barrier of the reaction between N_2 molecules and O atoms to form NO, i.e., ca. 3 eV, can be overcome by the vibrational energy of the N_2 molecules. As a result, the so-called Zeldovich mechanism stimulated by vibrational excitation,[31] will play the dominant role for producing NO in our gliding arc, while the N formed in this process can react with an O_2 molecule to form another NO:

$$O + N_2(v) \rightarrow NO + N,\ E_a \approx \Delta H \approx 3 \text{ eV/molec} \quad (3)$$

$N + O_2 \rightarrow NO + O$, $E_a \approx 0.3$ eV/molec, $\Delta H \approx -0.94$ eV/molec (4)

This will be further elaborated in the next section.

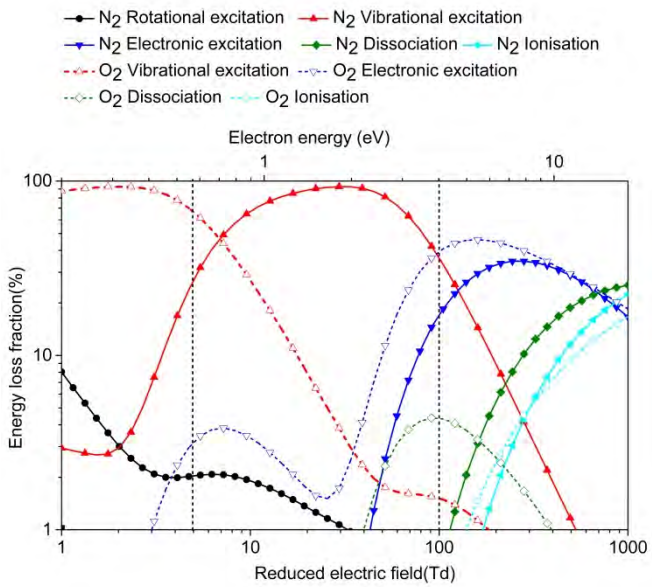

Figure 7. Fraction of electron energy transferred to different channels of excitation, as well as ionization and dissociation of N_2 and O_2, in a 50% N_2/ 50% O_2 mixture, as a function of the reduced electric field (E/n), as calculated from the corresponding cross sections of the electron impact reactions. The reactions with N_2 are indicated with solid lines, while the corresponding reactions with O_2 are plotted with dashed lines. The electron energies corresponding to the reduced electric field values are indicated at the top x-axis. The region between the two dashed vertical lines, indicating a reduced electric field between 5 and 100 Td, corresponds to the typical GA regime.

To demonstrate that the N_2 vibrational levels are indeed important in our gliding arc, we plot in figure 8 the vibrational distribution of N_2 in the gliding arc at four different times, i.e. at 5 µs (corresponding to the beginning of the first pulse; see supporting information for details), 15 µs, 25 µs and 35 µs (i.e. at the end of the first pulse). At the time instant of 5 µs, mainly the low vibrational levels are populated, due to electron excitation. When time evolves, the fast vibrational−vibrational (VV) relaxation, which is related to the vibrational energy exchange among two molecules in the same mode of vibration, leads to the establishment of a vibrational distribution where also the high-energy levels are gradually more populated, as is clear from figure 8. If the vibrational energy lost to translational degrees of freedom (VT relaxation processes) and chemical reactions would be neglected, the vibrational levels would show a Treanor distribution, i.e. an exponentially parabolic distribution function with a minimum value at intermediate vibrational levels [72]. However, when the chemical reactions of the vibrational levels are taken into account, the highest vibrational levels can overcome the reaction energy barrier. As a result, the destruction rate of the high vibrational levels is very large and the normalized vibrational distribution function shows a decreasing function with a larger slope with rising vibrational levels. By comparing the vibrational distribution functions calculated in the gliding arc with the equilibrium thermal distribution, calculated for a gas temperature of 1500 K, which is also plotted in figure 8, it is very obvious that the gliding arc discharge is highly vibrationally overpopulated throughout the entire power deposition pulse (or discharge cycle), explaining the important role of the N_2 vibrational levels in the NO formation in our gliding arc (see also next section).

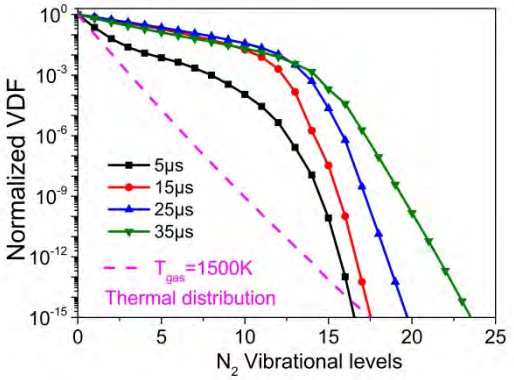

Figure 8. Normalized vibrational distribution function at different time instants of the first discharge pulse for a 50% N_2 / 50% O_2 mixture. The thermal distribution at the gas temperature of 1500 K is also presented for comparison.

Figure 9 illustrates the calculated vibrational temperature of N_2 as a function of time during the entire gliding arc discharge stage. It is defined as follows from the first vibrational level:

$$T_v = \frac{E_{v1}}{k_B ln(n_1/n_0)} \quad (5)$$

where E_{v1}/k_B = 3481 K is the energy of N_2v1 and n_1 and n_0 are the densities of N_2v1 and N_2 ground state, respectively. k_B is the Boltzmann constant.

It is clear that the vibrational temperature peaks at the maximum power deposition of one discharge pulse (see details in the supporting information), and drops again with the decrease of the power deposition. However, when the power drops to zero, the vibrational temperature is still higher than the gas temperature, because it cannot relax back to the gas temperature in the limited timescale before the start of the next power deposition pulse, when the vibrational temperature rises again. The maximum vibrational temperature, however, decreases with time, because both the power density and the electron number density decrease (see figure S5in the supporting information), and the electron energy transfer to vibrational energy by electron impact vibrational excitation is thus reduced. Near the end of the arc discharge stage, the vibrational temperature does not show a large variation during and in between two discharge pulses, but the vibrational temperature is still considerably higher than the gas temperature (i.e., about 5000 K vs 1000 K), indicating that the vibrational levels are overpopulated during the entire gliding arc cycle, and thus that the gliding arc is far from thermal equilibrium. Our calculated values of the vibrational temperature range from 4500 K to 8000 K, which is in general good agreement with experimental investigations [73]-[74] for a kilohertz AC air gliding arc at atmospheric pressure.

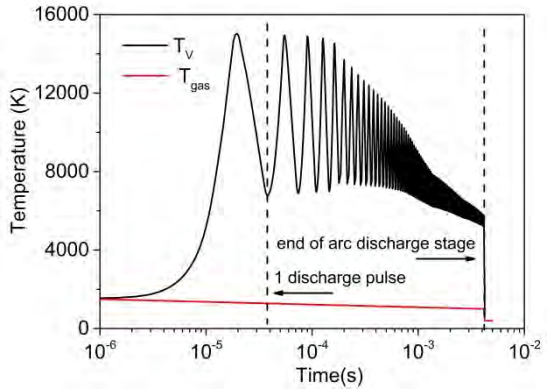

Figure 9. Vibrational temperature of the first vibrational state of N_2 as a function of time in the gliding arc discharge for a 50% N_2 / 50% O_2 mixture. The gas temperature is also presented for comparison.

It should be noted that not only the N_2 molecules but also the O_2 molecules are vibrationally excited in the gliding arc. The latter can also help to overcome the reaction energy barrier of the NO formation process (see reaction 4 above). However, as we can see from figure 7, the electron energy is more easily transferred to the vibrational energy of the N_2 molecules in the typical range of a gliding arc. Therefore, we only present here the results of the N_2 vibrational levels. In the next section we will try to elucidate the role of the various plasma chemical reactions and plasma species, and especially of the vibrational levels, on the actual NO_x synthesis in our gliding arc reactor.

Formation and loss processes of NO and NO_2

In order to better understand the influence of the N_2/O_2 feed ratio on the NO_x yield, we investigated the dominant reaction pathways for the formation and loss of NO and NO_2 for several N_2/O_2 feed ratios. This kinetic analysis was performed by looking at the time and volume integrated rates of the various processes for the total residence time of 5.0 ms (cf. figure S3in the supporting information).

Table 1lists the most important formation (F1-F6) and loss (L1-L5) processes for NO. In the supporting information(figure S6)we plot their time and volume integrated rates as a function of N_2/O_2 ratio, as well as the total formation and loss rate. As explained in the supporting information, some formation reactions are counteracted by some loss reactions. Hence, in order to investigate the net contribution of the forward and reverse reactions to the formation of NO, we plot in figure 10 the time and volume integrated net rates of the various NO formation processes as a function of N_2/O_2 ratio, as well as the total net formation rate.

Table 1. Overview of the most important formation and loss reactions for NO.

Formation processes		Loss processes	
F1	$O + N_2(v) \rightarrow NO + N$	L1	$N + NO \rightarrow O + N_2$
F2	$O + NO_2 \rightarrow NO + O_2$	L2	$O + NO \rightarrow NO_2$
F3	$N + O_2/O_2(v) \rightarrow NO + O$	L3	$NO + NO_2 + M \rightarrow N_2O_3 + M$
F4	$N_2O_3 + M \rightarrow NO + NO_2 + M$	L4	$NO_3 + NO \rightarrow NO_2 + NO_2$
F5	$N + NO_2 \rightarrow NO + NO$	L5	$NO_2^+ + NO \rightarrow NO^+ + NO_2$
F6	$NO_2^- + NO_2 \rightarrow NO_3^- + NO$		

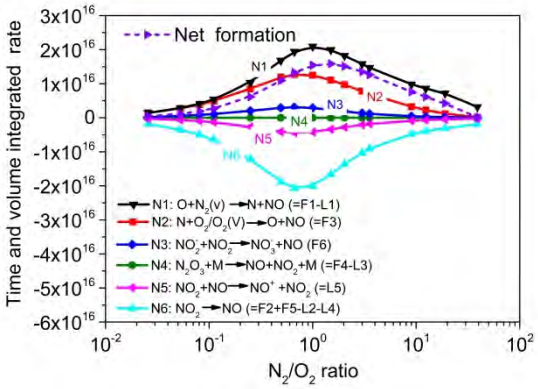

Figure 10. Time and volume integrated net rates of the various NO formation processes as a function of N_2/O_2 ratio, for a SEI of 1.4 kJ/L (or 0.35 eV/molec), as well as the total net formation rate.

Although the collision between oxygen atoms and NO_2 (i.e., $O + NO_2 \rightarrow NO + O_2$; F2) is the dominant formation mechanism of NO at low N_2/O_2 ratio, or high oxygen contents in the mixture, as shown in figure S6 of the supporting information, the reactions that proceed from NO_2 have an overall negative net contribution to the NO formation, as is very obvious from figure 10 (see N6) . This indicates that there is more formation of NO_2 from NO than vice versa, and reaction F2 does not count as net formation process of NO. In contrast, the rate of reaction F1 is 18 % higher than the rate of its reverse reaction L1 at the N_2/O_2 feed ratio of 1.0 (see figure S6), and thus, reaction F1 has a clear net contribution to NO formation (see N1). From this analysis we can therefore draw the following conclusion: the Zeldovich mechanism stimulated by vibrational excitation, i.e., $O + N_2(v) \rightarrow NO + N$ (F1), is the dominant production process of NO in the gliding arc, but the NO synthesis could be further enhanced if its reverse reaction (L1) could be reduced. Additionally, the second important formation process of NO is the reaction of N atoms with O_2 molecules (either in ground state or vibrational levels) (F3), so we should aim to steer the N atoms, formed in reaction F1, to react with O_2 molecules in reaction F3, instead of reacting with the NO molecules in the reverse reaction L1, in order to optimize the NO synthesis.

Table 2 lists the most important formation (F1-F4) and loss (L1-L6) processes for NO_2.Their time integrated rates are plotted in figure S7 of the supporting information, as a function of N_2/O_2 ratio, as well as the total formation and loss rate.

Table 2. Overview of the most important formation and loss reactions for NO_2.

Formation processes		Loss processes	
F1	$O + NO \rightarrow NO_2$	L1	$O + NO_2 \rightarrow NO + O_2$
F2	$N_2O_4 + M \rightarrow NO_2 + NO_2 + M$	L2	$NO_2 + NO_2 + M \rightarrow N_2O_4 + M$
F3	$NO_3 + NO \rightarrow NO_2 + NO_2$	L3	$NO_2 + NO_2 \rightarrow NO_3 + NO$
F4	$N_2O_3 + M \rightarrow NO + NO_2 + M$	L4	$NO + NO_2 + M \rightarrow N_2O_3 + M$
		L5	$N + NO_2 \rightarrow NO + NO$
		L6	$N + NO_2 \rightarrow O + N_2O$

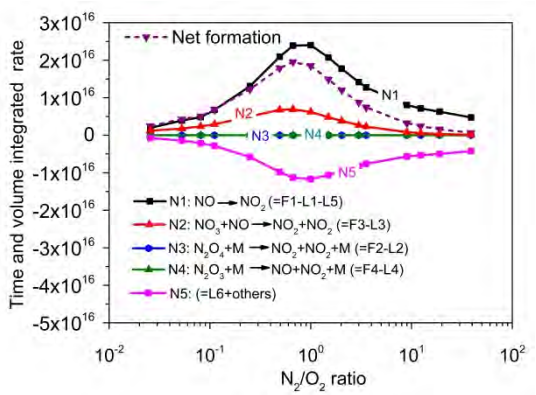

Figure 11. Time and volume integrated net rates of various NO_2 formation processes as a function of N_2/O_2 ratio, for a SEI of 1.4 kJ/L (or 0.35 eV/molec), as well as the total net formation rate.

Figure 11 shows the time and volume integrated net rates of the various NO_2 formation processes as a function of N_2/O_2 ratio. Although the reactions involving N_2O_4, i.e., F2 and L2, are the dominant formation and loss mechanism of NO_2 at N_2/O_2 feed ratio between 0.2 and 10, as shown in figure S7 of the supporting information, their absolute reaction rates are nearly balanced. Therefore, these reactions (combined as N3) have a negligible net contribution to the formation of NO_2. The same applies to the reaction N4, involving N_2O_3 (F4 and L4). Our calculations clearly indicate that the oxidation of NO via F1 is the most important net formation process of NO_2 (N1).

Overall reaction scheme of the NO_x chemistry

The data revealed by our 0D model allow us to compose an overall reaction scheme for the NO_x synthesis, as depicted schematically in figure 12. The 9.8 eV strong triple bond of N_2 is mainly broken by vibrational excitation, followed by the reaction of $N_2(v)$ with O atoms into NO and N (reaction 3 above).The N atoms subsequently react with O_2 molecules to form a second NO and a new O atom (reaction 4 above). The reaction chain is closed when the new O atom reacts with the next vibrationally excited N_2 molecule. Overall, NO is thus mainly produced by the non-thermal Zeldovich mechanism stimulated by vibrational excitation in the gliding arc. Indeed, the average electron energy in the gliding arc is in the range of 0.6-4.0 eV, which results in about 50-90 % electron energy transfer to N_2 vibrational excitation (see figure 7 above), while VV relaxation further populates the higher N_2 vibrational levels. The latter help to overcome the high reaction energy barrier of the Zeldovich reaction and promote the production of NO. Therefore, it is crucial to tune the reduced electric field (E/n) in the gliding arc, to establish an energy efficient way of NO production by the non-equilibrium plasma.

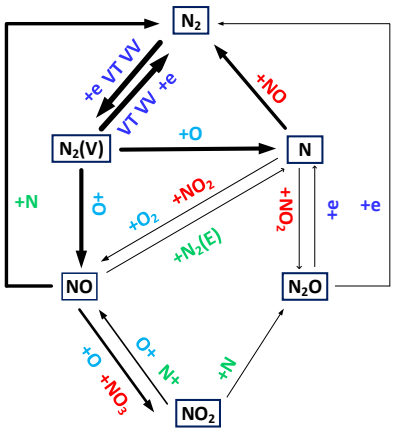

Figure 12. Reaction scheme to illustrate the main pathways of the NO_x chemistry in the gliding arc as predicted by our model. The thickness of the arrows corresponds to the importance of the reactions for a 50% N_2 / 50% O_2 mixture. For instance, the thickness of the arrow from $N_2(v)$ to NO corresponds to a time and volume integrated rate of 1.37×10^{17}.$N_2(E)$ indicates the sum of all the electronically excited N_2 molecules.

Our simulations indicate that for a total gliding arc cycle, a local NO_x concentration as high as 20 % can be reached within the gliding arc volume. A large fraction of the produced NO is, however, readily destroyed upon impact with N atoms in the active plasma zone (see also figure 12). By artificially setting the reaction rate of L1: N+NO→O+N_2 as zero, our calculation brings a much higher NO yield of 24588ppm_v with a N_2/O_2 feed ratio of 1, which is around 5 times of the yield obtained in fig.1 by taking into account this reaction. This clearly shows that suppressing the loss processes of L1 will enhance the NO_x yield and hence the overall energy efficiency. The reverse reaction ($N + NO \rightarrow O + N_2$) indeed competes with the propagation($N + O_2/O_2(v) \rightarrow NO + O$) of the Zeldovich chain, and it is able to terminate the chain when the NO concentration becomes high in the active discharge zone. This seriously restricts the yield of NO synthesis in our gliding arc. As a result, we should look for ways of suppressing the reverse reaction ($N + NO \rightarrow O + N_2$) or promoting the reaction $N + O_2/O_2(v) \rightarrow NO + O$, in order to increase the NO yield and hence improve the energy efficiency. For example, at a fixed SEI, by increasing the gas flow rate, the gas velocity becomes larger than the arc velocity and a larger amount of feed gas will be exposed to the plasma. The local NO concentration inside the arc would then decrease, but the overall NO yield and hence the energy efficiency would rise. Our experimental results for the NO_x concentration versus SEI indeed show that higher flow rates can produce higher NO_x concentrations at a fixed SEI. This shows the high potential of the gliding arc discharge for NO_x production at higher flow rates.
The promotion of the reaction $N + O_2/O_2(v) \rightarrow NO + O$ can be reached when making use of hot N atoms. Indeed, the vibrational energy of $N_2(v)$ is higher than the activation energy of the reaction $O + N_2(v) \rightarrow NO + N$ (i.e., 3.0 eV) for vibrational levels above v12, which corresponds to a vibrational energy of 3.2 eV. Thus, a fraction of the vibrational energy released goes into translational energy of the N atoms (so-called hot N atoms) and assists in the reaction $N + O_2/O_2(v) \rightarrow NO + O$, by increasing the rate coefficient of this reaction, and therefore, the

NO yield can be enhanced. It is shown in literature [75] that increasing the oxygen content in the mixture can help to enhance this effect and promote the reaction $N + O_2/O_2(v) \rightarrow NO + O$.

Our reaction scheme also shows that NO_2 is mainly formed by oxidation of NO upon reaction with O atoms, while it mainly reacts back into NO upon reaction with either O or N atoms, at high or low oxygen contents, respectively. The main channel responsible for the formation of O atoms, which are important to initiate the Zeldovich mechanism via $O + N_2(v) \rightarrow NO + N$, is electron impact dissociation of O_2 molecules.

Because the N atoms are lost rapidly via the reaction$N + NO \rightarrow O + N_2$, as well as by reactions with NO_2, our calculations indicate that the overall N concentration is never more than 0.1 %. For this reason, N_2O, which is mainly produced upon reaction between N atoms and NO_2 (reaction L6 in Table 2), has only a minor concentration in the whole gliding arc cycle compared with NO and NO_2. This is in qualitative agreement with our experiments, since no N_2O was detected.

As mentioned above, the industrial scale Haber–Bosch process still has a lower energy consumption, i.e. 0.48 MJ/mol N, so it is clear that major efforts should be taken gliding arc plasma-based N-fixation to further increase the yield and decrease the energy consumption, in order to become competitive with the industrial scale H-B process. Computer simulations, as presented here, can help to improve the process, as they elucidate the limiting factors for energy-efficient NO_x synthesis, and thus they can help to provide solutions to overcome these limitations.

On the other hand, it is important to realize that more and more electrical energy nowadays is produced from renewable energy sources (wind or solar), and this trend will continue in the coming years. As renewable energy sources often suffer from fluctuating peak powers (e.g., on windy or sunny days) when the electricity is in principle “for free”, our high frequency pulsed gliding arc plasma can be very useful for peak shaving, as it is very flexible and can be switched on and off easily, so we expect that it will be very suitable for N-fixation by NO_x synthesis using renewable energy. Furthermore, as an instantaneous “on-and-off” technique, the gliding arc based nitrogen fixation can be stopped and started more easily than the Haber-Bosch process, making it possible for farmers in remote locations to locally generate the necessary nitrogenous fertilizers out of “thin air” just using small scale plants. This application of gliding arc technology is very promising, especially in regions where there exist a wealth of under-used wind and solar resources, which offer farmers a new source of revenue from their land – a renewable alternative to conventional nitrogenous fertilizers that is compatible with growing crops because of its high operation flexibility.

Conclusions

The purpose of this work was to obtain a better understanding of the N-fixation process via NO_x synthesis in a gliding arc plasma, by means of combined experiments and a zero-dimensional kinetics model. We compared our experimental data with the model predictions and obtained reasonable agreement for the NO, NO_2, and total NO_x yield, the NO and NO_2 selectivity, the energy consumption and energy efficiency, for the entire range of N_2/O_2 feed ratios in the mixture. This indicates that our model can provide a realistic picture of the plasma chemistry and can be used to elucidate the dominant reaction pathways for the NO_x synthesis.

Our study clearly reveals that vibrational excitation of N_2 can help to overcome the reaction energy barrier of the non-thermal Zeldovich mechanism: $O + N_2(v) \rightarrow NO + N$,and can thus significantly enhance the production of NO. This provides an energy efficient pathway for NO formation in the gliding arc. Furthermore, our simulation shows that the most important reaction for NO_2 formation is oxidation of NO by O atoms:$O + NO \rightarrow NO_2$.

We also compared our results with those of thermal NO_x synthesis, as well as with results of other types of plasmas. The NO_x yield and energy efficiency obtained in our gliding arc are much higher than the thermal values, due to the non-equilibrium properties of the plasma, as the chemistry of the conversion process is induced by energetic electrons. When compared to other types of plasmas, we can conclude that the gliding arc is a very promising candidate for potential industrial scale N-fixation, but the energy consumption achieved in this study is still much higher than the benchmark, i.e., the industrial Haber-Bosch process. Therefore, it is clear that the NO_x synthesis in the gliding arc should be further improved, e.g., by operating at conditions where the reverse reaction $N + NO \rightarrow O + N_2$ is suppressed or where the reaction $N + O_2/O_2(v) \rightarrow NO + O$ is promoted, as our simulations indicate that these processes currently limit the NO_x formation.

In general we can conclude that our model allows us to gain better insights into the entire process of NO_x formation, which enables us to propose solutions for improving the gliding arc based NO_x synthesis processes in the future. One example could be to actively tune the reduced electric field (i.e.,E/nratio) by optimizing the reactor electrical operational parameters, to promote the vibrational excitation and selectively deliver energy to the Zeldovich chemical reaction of NO synthesis via an energy efficient way. Another example could be to improve the reactor geometry and optimize the flow conditions to expose the maximum amount of feed gas to the gliding arc.

Furthermore, Compared with the world-scale business case Haber-Bosch (which plasma will not replace at present stage),if electricity from sustainable energy sources is used, the intrinsic potential of gliding arc based nitrogen fixation processes promises an promising opportunity of producing fertilizer in remote locations. This comes up with realistic scenarios of entering a cutting-edge innovation in new business cases of plasma agriculture.

With the addition of water, an electric discharge in humid air produces reactive species and presents highly acid and oxidizing properties towards aqueous solutes.**Error! Reference source not found.** Besides the production of nitrogen fertilizers via the production of nitrate, these chemical effects which result from the plasma processing of aqueous solutes depend on the involved active particles and their population and properties in

the plasma gas, can also be used for various practical applications, for example, the removal of major pollutants from waste waters.[77] However, the interaction mechanism of water vapour with air (N_2/O_2) is not yet precisely clarified. Our current work shows the NO_x formation by the dehumidified air gliding arc strongly depends on the composition of the feeding gas, where the nature of the interactions, such as vibrational molecular excitation between the constituents, are very important. Therefore, identifying the role of different species especially their excited states and clarifying the underlying chemistry under different humidity contents will help propose solutions on how to enhance nitrate formation and improve the applied work via humid air gliding arc. We will devote much attention to this issue in our future work.

Experimental Section

Experimental studies

The experiments were carried out at atmospheric pressure in a milli-scale gliding arc reactor. This is a two-dimensional flat reactor in which the gas flow enters through a nozzle at the bottom of the reactor (see figure 13(a)). The reactor consists of two thin diverging knife-shaped molybdenum electrodes with thickness of 1.0 mm and height of 195 mm. The width of the reactor is 135 mm with narrowest discharge gap of 1.3 mm. A schematic diagram of the experimental set-up with milli-scale gliding arc reactor is also shown in figure 13(b). One of the electrodes is connected to the high voltage source and the other electrode is grounded. The reactor is powered by a customized Xenionik EP 4000 AC power supply. The applied high voltage and current are measured by a high voltage probe (Tektronix P6015A) and a current sense resistor of 5 Ω, respectively. All electrical signals are recorded using a USB powered four channel PC Oscilloscope (PicoScope R 3000).

Air and O_2 (Linde Gas, 99.9 %) were fed into the reactor using mass flow controllers (Bronkhorst) and no preheating of the gas occurred. The products were analysed using a Fourier Transform Infrared Spectrophotometer (SHIMADZU, IRTracer-100) at a resolution of 0.5 cm^{-1} and the gas cell is equipped with CaF_2 windows (Specac, Storm Series). NO and NO_2 were the only products detected and their concentrations were determined from the adsorption bands at 1900 cm^{-1} and 1630 cm^{-1}, respectively, using a series of calibration gas mixtures. The reported NO and NO_2 selectivity was calculated using Eq. 6:

$$NO\ selectivity = \frac{NO\ concentration}{concentration\ of\ (NO+NO_2)}$$

$$NO_2\ selectivity = \frac{NO_2\ concentration}{concentration\ of\ (NO+NO_2)} \qquad (6)$$

The arc dynamics in the plasma reactor is obtained using high speed imaging. This helps us to compute the gliding arc (GA) lifetime, GA velocity, GA propagation height and GA processing time, all of which are used as input in the model (see the supporting information).

The performance of the milli-scale gliding arc reactor was investigated at a constant flow rate of 2 L/min, pulse width (25 µs) and amplitude (70 Vpk–pk), and by varying the feed ratio of Air/O_2, yielding N_2/O_2 ratios of 0.25–4.All the experiments were performed 4 times and averages of at least 100 V-I cycles were used to obtain the final power consumption value. The influence of different flow rates, pulse widths and amplitudes on the NO_x yields was investigated in previous work[37]and is beyond the scope of our current work. We tested that Air+O_2 and N_2+O_2 feed gas mixtures with the same ratio of N_2/O_2 gave very similar concentrations of NO_x as well as selectivity towards NO, indicating that the minor components in air, such as argon and carbon dioxide, have limited influence on the NO_x(i.e., NO + NO_2) yield. Therefore, for simplicity, we assume the air is composed of N_2/O_2 = 79:21 in our simulation mentioned below.

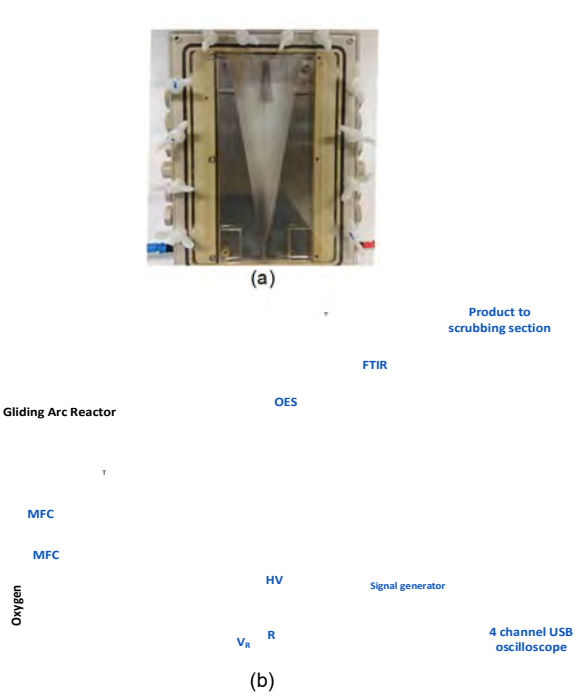

Figure 13. Reactor geometry (a) and schematic diagram of the experimental set-up (b)

The total plasma power (P_{plasma}), specific energy input (SEI), and energy consumption per mole of NO_x are defined by Eqs. (7)–(9), respectively.

$$P_{plasma}(W) = f\int_0^{t=tpulse} V_{GA} \times I_{GA}\,dt \qquad (7)$$

$$\text{Specific Energy Input (SEI; J/L)} = \frac{P_{plasma}(W)*60\ (s/min)}{Gas\ Feed\ Flow\ rate\ (L/min)} \qquad (8)$$

$$\text{Energy consumption}\left(\frac{\text{J}}{\text{mole}}\right) = \frac{P_{plasma}(W)+p_{gp}(W)}{Moles\ of\ NO_x Produced\ per\ second(mole/s)} \qquad (9)$$

Where t_{pulse} is the time span of a pulse (s) and *f* is the frequency of the pulses (Hz). $P_{gp}$is the power consumption used to prepare the pure oxygen gas via air separation.

$$Pgp(W) = \frac{Oxygen\ Flow\ rate\left(\frac{L}{min}\right)*Oxygen\ specfic\ power\ for\ air\ separation\left(\frac{W}{L}\right)}{60\ (s/min)} \qquad (10)$$

Where oxygen specific power for air separation is the power consumption needed to produce per standard litre oxygen gas and a value of 0.28 kW/L based on the Ref [78] is used here.

Likewise, the energy efficiency, η, is calculated as:

$$\eta(\%) = \frac{H_{NO_x}(J/mole)*Moles of NO_x Produced per second(mole/s)}{P_{plasma}(W)+Pgp(W)} \qquad (11)$$

Where H_{NO_x} is the standard formation enthalpy of 1 mole NO_x which is evaluated by equation (12),

$$H_{NO_x} = H_{NO} * S_{NO} + H_{NO2} * S_{NO2} \qquad (12)$$

Where H_{NO} and H_{NO_2} is the standard formation enthalpy of 1 mole

NO(90.3 kJ/mol) and NO_2 (33.1 kJ/mol), respectively, and S_{NO} and S_{NO2} is the selectivity of formed NO and NO_2 in the NO_x products.

Table 5. Major neutral reactions included in the model. The rate coefficients are in [$cm^3.s^{-1}$] or in [$cm^6.s^{-1}$] for the two-body and three-body reactions, respectively. Gas temperature T_g is in K.

Reaction	Rate coefficient	Ref.
$O + N_2 \rightarrow NO + N$	$3.0 \times 10^{-10}\exp(-38370/T_g)$	[61]
$O + NO_2 \rightarrow NO + O_2$	$6.51 \times 10^{-12}\exp(120.03/T_g)$	[81]
$N + NO \rightarrow O + N_2$	$8.20 \times 10^{-11}\exp(-410.03/T_g)$	[82]
$O + NO \rightarrow NO_2$	$3.02 \times 10^{-11}\exp(T_g/298.0)^{-0.75}$	[81]
$N + O_2 \rightarrow NO + O$	$4.47 \times 10^{-12}(T_g/300)\exp(-3270.0/T_g)$	[83]
$NO_3 + NO \rightarrow NO_2 + NO_2$	1.70×10^{-11}	[64]
$N + NO_2 \rightarrow NO + NO$	2.30×10^{-12}	[64]
$N + NO_2 \rightarrow O + N_2O$	1.40×10^{-12}	[82]
$NO_2 + NO_2 \rightarrow NO_3 + NO$	$4.5 \times 10^{-10}\exp(-18500.0/T_g)$	[61]

Computational studies

0D chemical kinetics model

In order to elucidate the underlying mechanisms of the gliding arc assisted NO_x synthesis in the above mentioned experimental setup, we developed a 0D plasma chemistry model, which allows to describe the behavior of a large number of species, and incorporate a large number of chemical reactions, with limited computational effort.

The zero-dimensional (0D) chemical kinetics model is based on solving balance equations for all the species densities, based on production and loss rates, as defined by the chemical reactions:

$$\frac{dn_i}{dt} = \sum_j \left\{ \left(a_{ij}^{(2)} - a_{ij}^{(1)}\right) k_j \prod_l n_l^{a_{lj}^{(1)}} \right\} \qquad (13)$$

where $a_{ij}^{(1)}$ and $a_{ij}^{(2)}$ are the stoichiometric coefficients of species *i*, at the left and right hand side of a reaction *j*, respectively, n_l is the species density at the left-hand side of the reaction, and k_j is the rate coefficient of reaction *j*. Transport processes such as diffusion are not considered; hence, the species densities are assumed to be constant in the entire simulation volume but they change with time. Nevertheless, this 0D model allows to describe the spatial dependence of the NO_x synthesis in the GA reactor, as explained in the supporting information.

The solution of the ordinary differential Eqs. (13)for the various plasma species is coupled with the Boltzmann equation, which is solved for the electron energy distribution function (EEDF). We use an existing code ZDPlasKin[79], which features an interface for the description of the plasma species and reactions, a solver for the set of differential Eqs.(13), and an integrated Boltzmann equation solver BOLSIG+.[80]

Plasma chemistry included in the model

The species taken into account in our model for the N_2/O_2 mixture are listed in Table 4. These species include various neutral molecules in the ground state, as well as several electronically and vibrationally excited levels, various radicals, positive and negative ions, and the electrons.

We pay special attention to the electronically and vibrationally excited states of N_2 and O_2, because they may become important under certain conditions. The detailed notations of the N_2 electronically excited levels are given in the table, while the vibrational levels of both N_2 and O_2 are indicated with (V). 15 vibrational levels are taken into account for O_2, while for N_2, 25 vibrationally excited levels are included. The populations of the higher levels are negligible, as was demonstrated in figure 8.

All these species undergo a large number of chemical reactions, i.e., electron impact collisions with neutral species, leading to excitation, ionization, dissociation and electron attachment, electron−ion recombination reactions, as well as many heavy-particle chemical reactions (i.e., ion-ion, ion-neutral and neutral-neutral reactions).

The chemistry set used in this model is mostly based on the models recently developed within our group, and validated for a microwave discharge [49]and a DBD discharge [50]in a CO_2/N_2 mixture. The corresponding rate coefficients, and the references where these data were adopted from, are listed in the supporting information of the previous work [49]. Some adjustments to the major neutral reactions involving NO_x were made and their corresponding rate constants are listed in Table 5. The first and fifth reaction do not only apply to N_2 and O_2 molecules in the ground state, respectively, but also to vibrational levels, with the rate coefficients adapted, as elaborated in the supporting information.

Because the vibrational energy can help overcome the activation energy barrier of the reaction and thus increase the reaction rate constant, we present in the supporting information in detail the reactions of the vibrational levels, i.e. electron impact excitation, vibrational energy exchange (VT and VV relaxation) reactions and chemical reactions (see section 1: Treatment of the vibrational level in the supporting information).

Acknowledgements

This research was supported by the European Marie Skłodowska-Curie Individual Fellowship “GlidArc” within Horizon 2020 (Grant No.657304), by the FWO project (grant G.0383.16N) and by the EU project MAPSYN: Microwave, Acoustic and Plasma assisted SYNthesis, under the grant agreement no. CP-IP 309376 of the European Community’s Seventh Framework Program. The calculations were performed using the Turing HPC infrastructure at the CalcUA core facility of the Universiteit Antwerpen (UAntwerpen), a division of the Flemish Supercomputer Center VSC, funded by the Hercules Foundation, the Flemish Government (department EWI) and the UAntwerpen.

Table 4. List of species included in the model for the N_2/O_2 gas mixture.

Ground neutral species	Charged species	Excited species
N_2, N	N^+, N_2^+, N_3^+, N_4^+	$N_2(A^3\Sigma_u^+)$, $N_2(B^3\Pi_g)$,$N_2(W^3\Delta_u)$, $N_2(B'^3\Sigma_u^-)$, $N_2(C^3\Pi_u)$, $N_2(E^3\Sigma_g^+)$, $N_2(a'^1\Sigma_u^-)$, $N_2(a^1\Pi_g)$, $N_2(a''^1\Sigma_g^+)$, $N_2(w^1\Delta_u)$, N_2(V1-V25), N(2D), N(2P)
O_2, O_3, O	O^+, O_2^+, O_4^+, O^-,O_2^-,O_3^-, O_4^-	O_2(V1-V15), O_2(E1)[a], O_2(E2)[b]
N_2O, N_2O_4, N_2O_5, NO,NO_2, NO_3	NO^+, N_2O^+, NO_2^+,NO^-, N_2O^-, NO_2^-, NO_3, $O_2^+N_2$ electrons	

[a] O_2(E1) = sum of the $A^1\Delta$and $b^1\Sigma$states
[b] O_2(E2) = $O_2(B^3\Sigma)$ and higher triplet states

Keywords: nitrogen fixation • gliding arc • NO_x synthesis• plasma chemistry• energy efficiency

[1] B.S. Patil, Q. Wang, V. Hessel,Jüergen. Lang,*Catal. Today* **2015***, 256,* 49–66.

[2] N. Cherkasov, A.O. Ibhadon, P. Fitzpatrick, *Chem. Eng. Process.***2015**,*90*, 24–33.

[3] http://energy.globaldata.com/media-center/press-releases/oil-and-gas/global-ammonia-capacity-to-reach-almost-250-million-tons-per-year-by-2018-says-globaldata.

[4] J. N. Galloway, *Environ. Pollut.***1998**,*102*, 15–24.

[5] Y. Tanabe, Y. Nishibayashi, *Coord. Chem. Rev.***2013**,*257*, 2551–2564.

[6] R. R. Schrock, *Proc. Natl. Acad. Sci. U. S. A.***2006**, *103*, 17087.

[7] A. Anastasopoulou, Q. Wang, V. Hessel, Jüergen Lang, *Processes* **2014**, *2*, 694-710.

[8] V. Hessel, G. Cravotto, P. Fitzpatrick, B. S. Patil, Jüergen Lang, W. Bonrath*, Chem. Eng. Process.***2013**,*71*, 19–30.

[9] R. H. Burris, G. P. Roberts, *Annu. Rev. Nutr.***1993**, *13*, 317–335.

[10] T. Bazhenova, A. Shilov, *Coord. Chem. Rev.***1995**,*144*, 69–145.

[11] M. E. Vol'pin, V. B. Shur, M. A. Ilatovskaya*, Bull. Acad. Sci. USSR Div. Chem. Sci.* **1964**,*13*,1644.

[12] D. Rapakoulias, S. Cavadias, J. Amouroux, *Revue de Physique Appliquée (Paris)* **1980**,*15*, 1261–1265.

[13] I. Pollo, *Matematyka-Fizyka-Chemia***1978**,*20*, 102–108.

[14] J. Krop, I. Pollo,*Chemia* **1980**, *633*, 25–33.

[15] B. Mutel, O. Dessaux, P. Goudmand, *Rev. Phys. Appl.***1984**,*19*, 461–464.

[16] V. D. Rusanov, A. A. Fridman, G.V. Sholin, *Sov. Phys. Usp.***1981**,*24*, 447–474.

[17] A. Czernichowski, *Pure & Appl. Chem.***1994**, *66*, 1301-1310

[18] A. Indarto, D. R. Yang, J. W. Choi, H. Lee,H. K. Song, *J. Hazard. Mater.***2007**, *146*, 309–315.

[19] T. Nunnally, K. Gutsol, A. Rabinovich, A. Fridman, A. Gutsol,A. Kemoun*, J. Phys. D. Appl. Phys.***2011**, *44*, 274009.

[20] X. Tao, M. Bai, X. Li, H. Long, S. Shang, Y. Yin,X. Dai, *Prog. Energy Combust. Sci.***2011**, *37*, 113–124.

[21] G. Petitpas, J.D. Rollier, A. Darmon, J. Gonzalez-Aguilar, R. Metkemeijer,L. Fulcheri, *Int. J. Hydrogen Energy***2007**, *32*, 2848–2867.

[22] C. S. Kalra, A. F. Gutsol, A. A. Fridman, *IEEE Trans. Plasma Sci.* **2005**,*33*, 32-41.

[23] T. Sreethawong, P. Thakonpatthanakun,S. Chavadej, *Int. J. Hydrogen Energy***2007**,*32*, 1067-1079.

[24] Y. N. Chun,H. O. Song, *Energy Sources. A: Recov. Util. Environ. Eff.***2008**,*30*, 1202-1212.

[25] T. Nunnally, K. Gutsol, A. Rabinovich, A. Fridman, A.Starikovsky,A. Gutsol, *J. Phys. D: Appl. Phys.***2011**,*44*, 274009.

[26] D. R. Yang, J. W. Choi, H. Lee, H. K. Song,*J. Hazard. Mater.***2007**,*146*, 309-315.

[27] S. C. Kim, M. S. Lim, Y. N. Chum,*Plasma Chem Plasma Process***2014**,*34*, 125-143.

[28] H. Zhang, X. D. Li, F. S. Zhu, K. F. Cen, C. M. Du, X. Tu*, Chem. Eng. J.***2017**,*310*, 114-119.

[29] H. Zhang, C. M. Du, A. J. Wu, Z. Bo, J. H. Yan, X. D. Li, *Int. J. Hydrogen Energy***2014**, 39, 12620-12635.

[30] A. A. Fridman, S. Nester, L. A .Kennedy, A. Saveliev, O. Mutaf-Yardimci, *Prog. Energy Combust. Sci.***1999**,*25*, 211-231.

[31] A. Fridman, Plasma Chemistry, Cambridge University Press, New York, 2008.

[32] R. Burlica, M. J. Kirkpatrick, B. R. Locke,*J. Electrostatics***2016**,*64*, 35–43.

[33] J. M. Cormier, O. Aubry, A. Khacef, *NATO Secur. Sci. Ser. A Chem. Biol.* **2008**, 125-134.

[34] Z. Czekalska,*Arch.Combust.***2010**, *30*, 337–346.

[35] Z. Bo, J. Yan, X. D. Li, Y. Chi, K. F. Cen, *J. Hazard. Mater.* **2009**,*166*, 1210–1216.

[36] J. Yang, T. Y. Lia, C. S. Zhong, X. X. Guan,C. Hu, *J. Electrochem. Soc.***2016**,*163*, E288-E292.

[37] B. S. Patil, J. R. Palau, V. Hessel, Jüergen Lang, Q. Wang, *Plasma Chem Plasma Process***2016**, *36*, 241–257.

[38] J. Amouroux, S. Cavadias, D. Rapakoulias, *Rev. Phys. Appl.***1979**,*14*, 969–976.

[39] X. Tu, H. J. Gallon, J. C. Whitehead, *IEEE Trans. Plasma Sci.***2011**,*39*, 2900-2901.

[40] X. Tu, J. C. Whitehead,*Int. J. Hydrogen Energy***2004**,*39*, 9658-9669.

[41] S. Pellerin, J. M. Cormier, F. Richard, K.Musiol, J. Chapelle,*J. Phys. D: Appl. Phys.***1999**,*32*, 891–897.

[42] I. V. Kuznetsova, N. Y. Kalashnikov, A. F. Gutsol, A. A. Fridman,L. A. Kennedy, *J. Appl. Phys.***2002**, *92*, 4231–4237.

[43] A. Czernichowski, H. Nassar, A. Ranaivosoloarimanana,*Acta Physic A Polonica A***1996**, *89*, 595-596.

[44] O. Mutaf-Yardimci, A. V. Saveliev, A. A. Fridman,L. A. Kennedy, *J. Appl. Phys.***1999**, *84*, 1062-1641.

[45] T. Kozák, A. Bogaerts, Plasma Sources Sci. Technol. **2014**, *23*, 045004.

[46] T. Kozák, A. Bogaerts, Plasma Sources Sci. Technol. **2015**,*24*, 015024.

[47] R. Aerts, W. Somers, A. Bogaerts, *ChemSusChem***2015**, 8, 702-716.

[48] R. Snoeckx, R. Aerts, X. Tu, A. Bogaerts, *J. Phys. Chem. C***2013**,*117*, 4957-4970.

[49] S.Heijkers, R. Snoeckx, T. Kozák, T. Silva, T. Godfroid, N. Britun, R. Snyders, A. Bogaerts, *J. Phys. Chem. C***2015**,*119*, 12815–12828.

[50] R. Snoeckx, S. Heijkers, K. Van Wesenbeeck, S. Lenaerts, A. Bogaerts, *Energy Environ. Sci.***2016**,*9*, 999—1011.

[51] W. Z. Wang,A. Bogaerts, *Plasma Sources Sci. Technol.***2016**, 25, 055025.

[52] F. Richard, J. M. Cormier, S. Pellerin, J. Chapelle, *J. Appl. Phys.***1996**, *79*, 2245–2250.

[53] S. Pellerin, F. Richard, J. Chapelle, J. M. Cormier,K. Musiol, *J. Phys. D: Appl. Phys.* **2000**, *33*, 2407-2419.

[54] St. Kolev and A. Bogaerts, *Plasma Sources Sci. Technol.***2015**,*24*, 015025.

[55] St. Kolev and A. Bogaerts, *Plasma Sources Sci. Technol.***2015**,*25*, 035014.

[56] G. Trenchev, St. Kolev, A. Bogaerts, *Plasma Sources Sci. Technol.***2015**, 24, 015025.

[57] S. R. Sun, St. Kolev, H. X. Wang, A. Bogaerts, *Plasma Sources Sci. Technol.***2016**,*26*, 015003.

[58] S. R. Sun, H. X. Wang, D. H. Mei, X. Tu, A. Bogaerts, *Journal of CO_2 Utilization***2017**,*17,* 220–234.

[59] W. Z. Wang, A. Berthelot, St. Kolev, X. Tu,A Bogaerts,*Plasma Sources Sci. Technol.***2016**, *25*, 065012.

[60] V. Guerra, J. Loureiro, *J. Phys. D: Appl. Phys.***1995**,*28*, 1903-1918.

[61] M. Capitelli, C. M. Ferreira, B. F. Gordiets, A. I. Osipov, Plasma kinetics in atmospheric gases, Springer, Berlin, 2000.

[62] B. F. Gordiets, C. M. Ferreira, V. L. Guerra, J.M.A.H. Loureiro, J. Nahorny, D. Pagnon, M. Touzeau, M. Vialle,*IEEE Trans. Plasma Sci.* **1995**, *23*, 750-768.

[63] V. Guerra, P. A. Sá, J. Loureiro, *Eur. Phys. J. Appl. Phys.***2004**,*28*, 125-152.

[64] I. A. Kossyi, A. Yu. Kostinsky, A. A. Matveyev, V. P. Silkov,*Plasma Source Sci. Technol.***1992**,*1*, 207-220.

[65] A. B. Murphy, J. Phys. D. Appl. Phys. **2001**, *34*, 51–173.

[66] M. Appl, *Ullmann's Encycl. Ind. Chem.* **2012**, 139–225.

[67] E. D. Mccollum, F. Daniels, Ind. Eng. Chem. 1923, 15, 1173–1175.

[68] W. S. Partridge, R. B. Parlin, B. J. Zwolinski, Ind. Eng. Chem. 1954, 46, 1468–1471.

[69] M. Rahman, V. Cooray, Opt. Laser Technol. 2003, 35, 543–546.

[70] W. L. Chameides, D. H. Stedman, R. R. Dickerson, D. W. Rusch, R. J. Cicerone, J. Atmos. Sci. 1977, 34,143–149.

[71] N. Rehbein, V. Cooray, J. Electrostatics 2001, 51–52, 333–339.

[72] C. E. Treanor, *J. Chem. Phys.***1968**, *48*, 1798−1807.
[73] T. L. Zhao, Y. Xu, Y. H. Song, X. S. Li, J. L. Liu, J. B. Liu, A. M. Zhu, *J. Phys. D: Appl. Phys.***2013**, *46*, 345201.
[74] J. Zhu, J. Gao, A. Ehn, Z. Li, M. Aldén, M. Salewski, Y. Kusano, Translational, rotational and vibrational temperatures of a gliding arc discharge at atmospheric pressure air. In R. Brandenburg, & L. Stollenwerk (Eds.), 14th International Symposium on High Pressure Low Temperature Plasma Chemistry: Book of Contributions, 2014, INP Greifswald.
[75] T. A. Grigorieva, A. A. Levitsky, S. O. Macheret, L. S. Polak, A. Fridman, A. Sov. Phys., High Energy Chem. (Khimia Vysokikh Energij) **1984**, *18*, 268-272.
[76] B. Benstaali, D. Moussa, A. Addou, J.-L. Brisset, *Eur. Phys. J. AP***1998**, *4*, 171-179.
[77] J. H. Yan, C. M. Du, X. D. Li, B. G. Cheron, M. J. Ni, K. F. Cen, *Plasma Chem Plasma Process*, **2006**, *26*, 31-41.
[78] W. Castle, *International Journal of Refrigeration***2002**, *25*, 158–172.
[79] S. Pancheshnyi, B. Eismann, G. Hagelaar, L. Pitchford, Computer code zdplaskin (University of Toulouse, LAPLACE, CNRS-UPS-INP, France) www.zdplaskin.laplace.univ-tlse.fr, 2008.
[80] G. J. M. Hagelaar,L. C. Pitchford,*Plasma Sources Sci. Technol.***2005**, *14*, 722–733.
[81] W. Tsang, J. T. Herron, *J. Phys. Chem. Ref. Data.***1991**,*20*, 609-663.
[82] M. A. A. Clyne, I. S.McDermid, *J. Chem. Soc.: Faraday Trans. I: Physical Chemistry in Condensed Phases***1975**, 71, 2189-2202.
[83] D. L. Baulch, C. J. Cobos, R. A. Cox, P. Frank, G. Hayman, Th. Just, J. A. Kerr, T. Murrells, M. J. Pilling, J. Troe, R. W. Walker, J. Warnatz, *Supplement I. J. Phys. Chem. Ref. Data***1994**,*23*, 847-1033.

Entry for the Table of Contents (Please choose one layout)

Layout 1:

FULL PAPER

Nitrogen fixation is gaining increasing interest due to its essential role in the nitrogen cycle of the biosphere. A gliding arc plasma has great potential for this purpose, however, the understanding of the underlying mechanisms is very limited. This work presents an extensive study elucidating the plasma chemistry by a combination of experiments and computations to provide the necessary insights for improving gliding arc based NO_x synthesis.

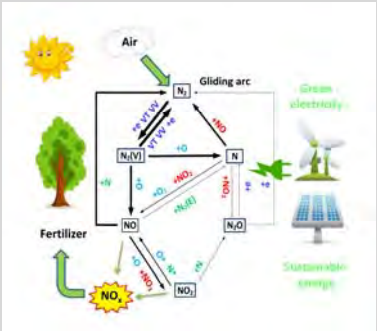

Weizong Wang, Bhaskar Patil, Stjin Heijkers, Volker Hessel and Annemie Bogaerts**

Page No. – Page No.

Nitrogen Fixation by Gliding Arc Plasma: Better Insight by Chemical Kinetics Modelling

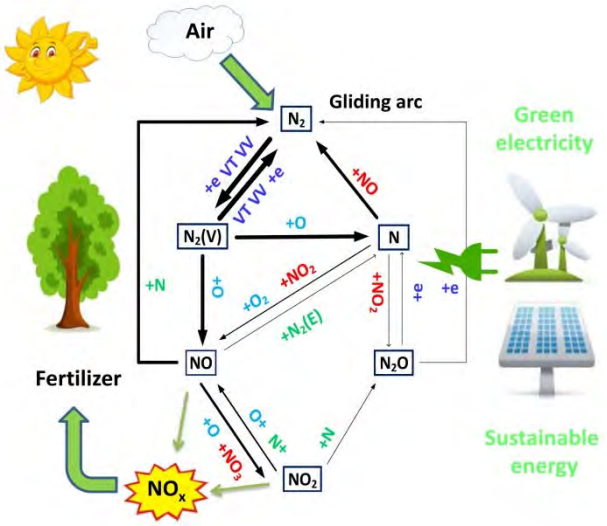

Table of Contents (enlarged)